NASA/TM–2019-220413

# Preliminary Nonlinear Structural Analysis of Advanced Composite Tow-Steered Shells with Large Geometric Imperfections

*Calvin P. Dobrin*
*Rutgers University, New Brunswick, New Jersey*

*K. Chauncey Wu and Bret K. Stanford*
*Langley Research Center, Hampton, Virginia*

October 2019

# NASA STI Program . . . in Profile

Since its founding, NASA has been dedicated to the advancement of aeronautics and space science. The NASA scientific and technical information (STI) program plays a key part in helping NASA maintain this important role.

The NASA STI program operates under the auspices of the Agency Chief Information Officer. It collects, organizes, provides for archiving, and disseminates NASA's STI. The NASA STI program provides access to the NTRS Registered and its public interface, the NASA Technical Reports Server, thus providing one of the largest collections of aeronautical and space science STI in the world. Results are published in both non-NASA channels and by NASA in the NASA STI Report Series, which includes the following report types:

- TECHNICAL PUBLICATION. Reports of completed research or a major significant phase of research that present the results of NASA Programs and include extensive data or theoretical analysis. Includes compila-tions of significant scientific and technical data and information deemed to be of continuing reference value. NASA counter-part of peer-reviewed formal professional papers but has less stringent limitations on manuscript length and extent of graphic presentations.

- TECHNICAL MEMORANDUM. Scientific and technical findings that are preliminary or of specialized interest, e.g., quick release reports, working papers, and bibliographies that contain minimal annotation. Does not contain extensive analysis.

- CONTRACTOR REPORT. Scientific and technical findings by NASA-sponsored contractors and grantees.

- CONFERENCE PUBLICATION. Collected papers from scientific and technical conferences, symposia, seminars, or other meetings sponsored or co-sponsored by NASA.

- SPECIAL PUBLICATION. Scientific, technical, or historical information from NASA programs, projects, and missions, often concerned with subjects having substantial public interest.

- TECHNICAL TRANSLATION. English-language translations of foreign scientific and technical material pertinent to NASA's mission.

Specialized services also include organizing and publishing research results, distributing specialized research announcements and feeds, providing information desk and personal search support, and enabling data exchange services.

For more information about the NASA STI program, see the following:

- Access the NASA STI program home page at http://www.sti.nasa.gov

- E-mail your question to help@sti.nasa.gov

- Phone the NASA STI Information Desk at 757-864-9658

- Write to:
  NASA STI Information Desk
  Mail Stop 148
  NASA Langley Research Center
  Hampton, VA 23681-2199

NASA/TM–2019-220413

# Preliminary Nonlinear Structural Analysis of Advanced Composite Tow-Steered Shells with Large Geometric Imperfections

*Calvin P. Dobrin*
*Rutgers University, New Brunswick, New Jersey*

*K. Chauncey Wu and Bret K. Stanford*
*Langley Research Center, Hampton, Virginia*

October 2019

# Preliminary Nonlinear Structural Analyses of Advanced Composite Tow-Steered Shells with Large Geometric Imperfections

Calvin P. Dobrin, K. Chauncey Wu and Bret K. Stanford
NASA Langley Research Center
Hampton, Virginia

## Abstract

The structural performance of two advanced composite tow-steered shells with and without tow overlaps, and with large geometric imperfections, are predicted using linear and geometrically nonlinear finite element analyses. These shells, 35 in. long and approximately 16.3 in. diameter, are fabricated using automated fiber placement from IM7/8552 graphite/epoxy prepreg. The 8-ply, $[\pm45/\pm\Theta]_s$ shell layup incorporates a steered fiber angle $\Theta$ that varies from 10 deg. to 45 deg. periodically over the shell circumference. Shell analysis models are evaluated using geometric imperfections normalized to ±1 shell wall thickness (±0.040 in.), which are then superposed and rotated incrementally around the shell longitudinal axis. Using these nominal imperfections, the shell prebuckling axial stiffnesses and buckling loads predicted with linear and nonlinear analyses are close to reference values from linear analyses with no imperfections. The linear and nonlinear analyses are then repeated for scaled imperfections that are larger by up to a factor of 10. For these larger imperfections, linear analyses predict reductions in axial stiffnesses and buckling loads of up to 5 and 30 percent, respectively, from reference values. The nonlinear analyses predict even larger reductions in axial stiffnesses and buckling loads of up to 10 and 55 percent, respectively.

## 1. Introduction

Fabrication of advanced composite structures incorporating tow steering, where continuous load-bearing fibers are oriented along curvilinear paths within individual plies, is enabled by automated composites manufacturing machinery (Ref. 1). Tailoring of the fiber angles in tow-steered laminates may offer improvements in structural performance and reduced weight over conventional straight-fiber composites (Ref. 2). To better assess the potential benefits of this class of advanced composites, two monocoque shells with tow-steered layups were designed (Ref. 3), fabricated using fiber placement (Ref. 4), and analyzed and tested in axial compression (Ref. 5), where good correlation was observed between linear finite element analysis (FEA) results and the shells' measured prebuckling axial stiffness and buckling loads.

In Ref. 6, very good test-analysis correlation was also observed for the predicted nonlinear load-displacement responses into deep postbuckling and back to zero load. Four distinct regions in the shells' load-displacement response were identified in these displacement-controlled tests and analyses. Starting at zero load and displacement, these regions are linear prebuckling, nonlinear postbuckling, nonlinear unloading, and finally linear unloading back to zero. Global buckling occurs between the linear prebuckling and nonlinear postbuckling regions.

An analytical study was performed in Ref. 7 using linear FEA to investigate the insensitivity of the shells' performance in more detail. In that study, measured geometric imperfections were superposed on finite element models of both shells, and successive linear FEA were performed as the imperfections were rotated at fixed intervals about the shell longitudinal axis. The analyses in

Ref. 7 showed that the shells' prebuckling stiffness and buckling load varied by at most +1 to –4 percent from reference values computed without imperfections.

The objective of this present research is to extend the analyses in Ref. 7 to further assess the structural performance of the two tow-steered shells both with and without overlaps, and with geometric imperfections that are first normalized to ±1 shell wall thickness amplitude and then scaled uniformly up to ±10 shell wall thicknesses. For each shell configuration, the prebuckling linear axial stiffness and the lowest global buckling load are computed using linear and geometrically nonlinear FEA. Postbuckling behavior of the shells after that initial buckling load was achieved is not a primary consideration in this study, and only shells without cutouts are assessed.

## 2. Tow-Steered Shells Description

The design and fabrication of the tow-steered shells evaluated in this study are discussed in detail in Refs. 3 and 4, respectively. These shells are fabricated from IM7/8552 graphite/epoxy prepreg slit tape (each 1/8-in. wide), using an automated fiber placement system (AFPS, Figure 1) that can deposit up to 24 slit tapes in each course, or pass of the AFPS. One shell is fabricated with full material overlapping between adjacent courses, so that the laminate thickness varies between 8 plies on the shell sides, increasing to 16 plies on the crown and keel. The second shell uses the AFPS capability to cut and add individual slit tapes to minimize overlaps and produce a near-uniform laminate thickness over the entire planform. These shells, with and without tow overlaps, respectively, are designated here as Shells A and B.
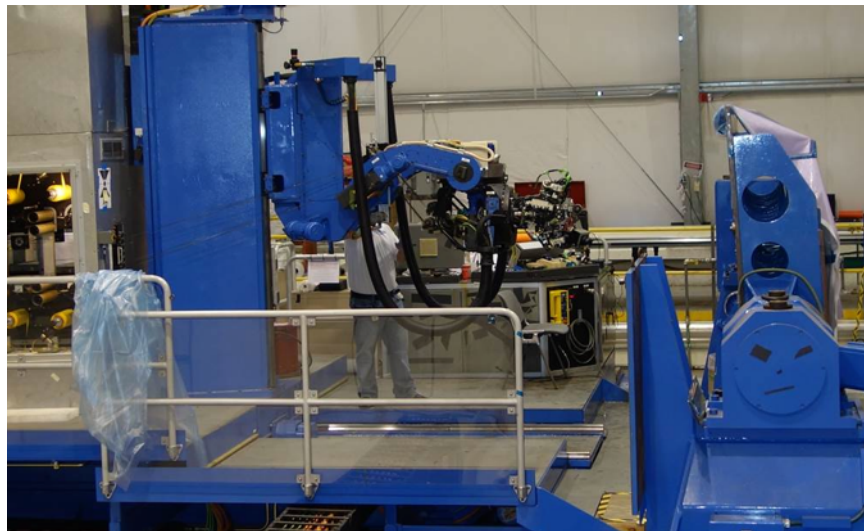


**Figure 1. Fiber placement system (Lockheed Martin/NCAM).**

Both tow-steered shells have a nominal 8-ply, $[\pm45/\pm\Theta]_s$ layup. The fiber angle $\Theta$ varies continuously along a constant-radius circular arc (Ref. 3) from $\Theta_0 = 10$ deg. on the shell crown, to $\Theta_1 = 45$ deg. on the shell side. This reference fiber path is shown as the blue line in the shell planform view in Figure 2, and spans one-quarter of the shell circumference (the red line in the figure). The reference fiber path is then mirrored about its endpoints to extend it into adjacent quadrants of the shell surface while still maintaining $C_0$ and $C_1$ continuity. This extended fiber path is then shifted axially to fully populate the entire shell planform, as shown in the figure. The axial shift increments between the extended fiber paths are defined so that no tow overlaps occur

on the shell sides, and to locate the resulting tow overlaps for Shell A toward the shell crown and keel.
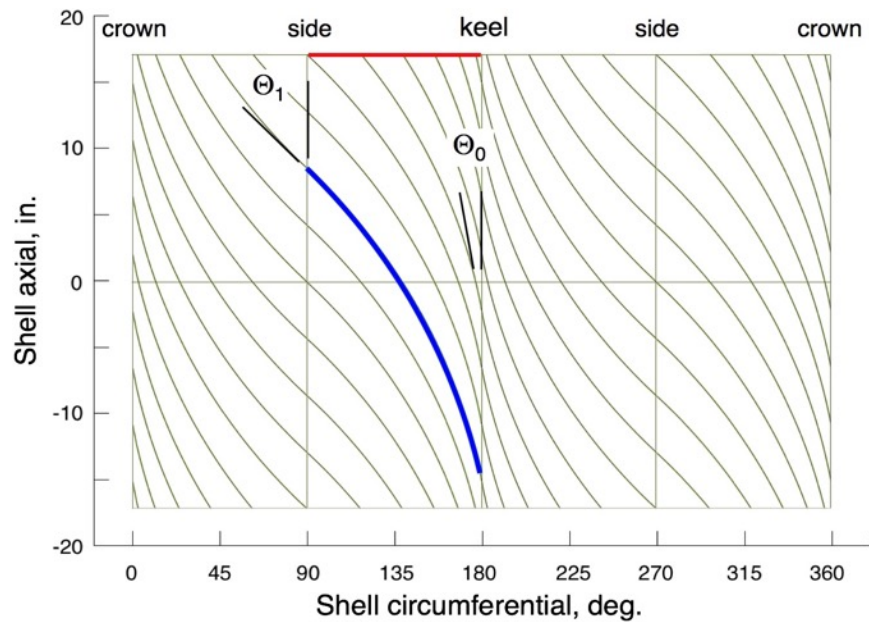


**Figure 2. Tow-steered ply course centerlines.**

To predict the laminate thicknesses for Shell A, the maximum 3-in. width of each tow course (24 tows x 1/8-in. tow width) is superposed on the fiber paths in Figure 2. The individual overlap patterns for each of the four tow-steered and four straight-fiber plies are integrated, and result in the laminate thickness patterns shown in Figure 3. The Shell A laminate thicknesses vary from 8 (blue) plies along the shell sides, to 16 (red) plies on the shell crown and keel. Intermediate laminate thicknesses of 10, 12, and 14 plies are indicated in the figure in green, yellow, and orange, respectively. In comparison, Shell B is predicted to have a uniform, 8-ply, laminate thickness.
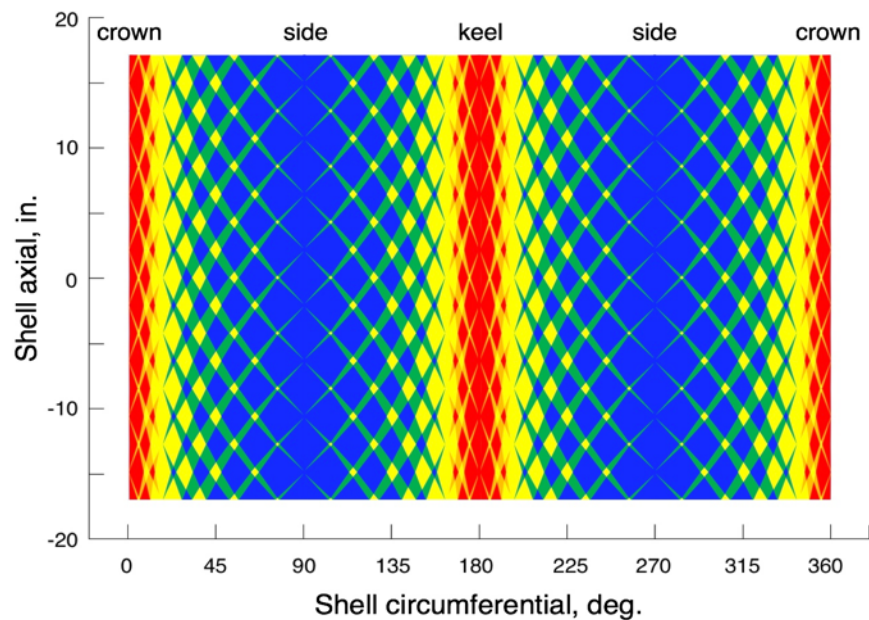


**Figure 3. Predicted Shell A laminate thicknesses.**

3

To prepare the shells for structural testing, epoxy potting is used to prevent local brooming failure during testing (Ref. 5), and is cast over the last 1 in. of both shell ends. After curing, the potted end surfaces of the shells are then machined flat and parallel to a 35 in. overall test length. Axial compression testing and supporting linear FEA are also described in Ref. 5, with measured prebuckling axial stiffnesses and buckling loads listed in Table 1.

**Table 1. Measured performance of tow-steered shells.**

| Performance metric | Shell A | Shell B |
|---|---|---|
| Prebuckling axial stiffness, klb/in. | 531.2 | 328.7 |
| Buckling load, klbs | 38.8 | 17.2 |

The instrumentation used to measure the shell structural behavior during testing includes a load cell permanently installed in the 300 klb-capacity electromechanical test stand, four linear variable displacement transducers to record the shell end shortening, and electrical resistance strain gauges to collect axial and lateral strains on the shell inner and outer surfaces. A digital interferometry system is also deployed for full-field, 3-dimensional, assessment of the shells' displacements and strains.

### 3. Shell Geometry Survey Results

The outer and inner surfaces of the cured shells are surveyed using a coordinate measuring machine, and their average inner diameter is measured at 16.290 inches (Ref. 4). The measured shell laminate thicknesses (Ref. 4), defined as the difference between the outer and inner shell surfaces and plotted in Figure 4, provide qualitative but not quantitative (i.e., direct one-to-one) comparisons with the predicted laminate thicknesses for Shells A and B. For example, the predicted laminate thicknesses for Shell A in Figure 3 compare well to the measured laminate thicknesses in Figure 4a, with similar thinner regions on the shell sides designated in blue, and thicker regions toward the crown and keel in red.
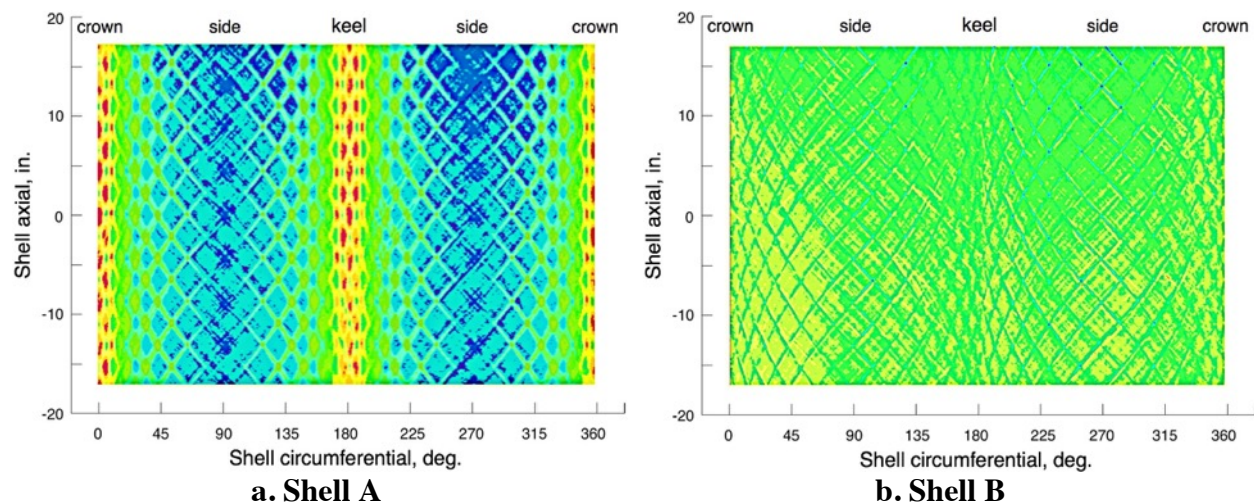


a. Shell A      b. Shell B
**Figure 4. Measured shell laminate thickness.**

Measured laminate thicknesses (Ref. 4) for Shell A vary from 0.032 to 0.086 in., with distinct lobes corresponding to discrete thicknesses of 8, 10, and 12 plies, and smaller lobes at 14 and 16 plies. The measured laminate thicknesses for Shell B vary from 0.022 to 0.059 in., with a mean

value of 0.039 in. While the measured Shell B thicknesses in Figure 4b are not uniform as predicted, they exhibit a relatively low coefficient of variation of 6.2 percent. For this study, the reference shell wall thickness of 0.040 in. is defined as the product of the nominal 0.005-in. ply thickness and the nominal 8-ply layup.

## 4. Normalized Geometric Imperfections

After surveying the cured shells' smooth inner surface using a coordinate measuring machine (Ref. 4), the shell geometric imperfections are then defined as the inner surface's deviations from a best-fit, right-circular cylinder, with a zero-mean value. After normalization by the reference shell wall thickness of 0.040 in., the measured geometric imperfections will range from +0.825 to −1.125 shell wall thicknesses for Shell A, and +1.475 to −1.225 shell wall thicknesses for Shell B. These measured imperfections were used extensively for the imperfection insensitivity analyses in Ref. 7. However, to reduce any possible bias in the present study's analysis results, these measured imperfection data are first normalized to amplitudes of ±1 shell wall thickness.

To normalize the measured imperfections, each imperfection dataset is first sorted into ascending order. Then, all positive values are divided by the maximum value, and all negative values are divided by the minimum value. These positive and negative subsets (now with maximum and minimum values of +1 and −1, respectively) are then concatenated, and the mean value of this combined dataset is computed and subtracted. This iterative process is repeated successively until the resulting mean value converges to a numeral zero (to at least 5 decimal places).

These normalized imperfections, now designated as the nominal A2 and B2 Imperfections with a scale factor SF = 1, are shown in Figure 5 with an orientation of $\Phi = 0$ deg. that corresponds to the as-measured orientation of the shells. The imperfections in Figure 5 have the same qualitative shapes reported in Ref. 4. The A2 Imperfections in Figure 5a are nearly symmetric about two orthogonal planes, while the B2 Imperfections in Figure 5b are more asymmetric.
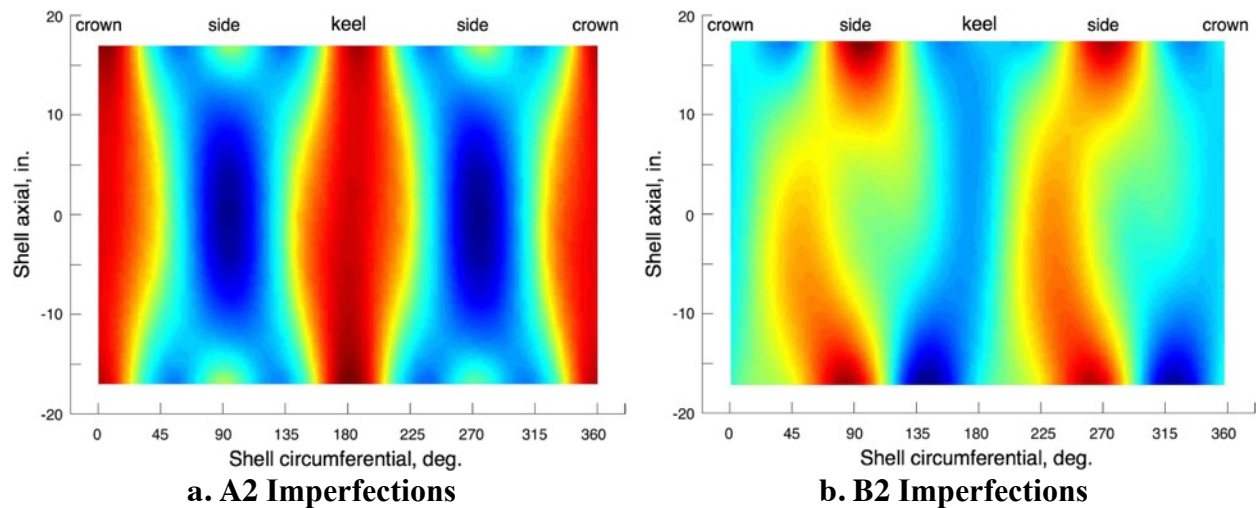


a. A2 Imperfections                    b. B2 Imperfections
Figure 5.  Normalized shell geometric imperfections.

## 5. Shell Finite Element Models

NASTRAN (Ref. 8) finite element models are developed for Shells A and B. A converged mesh with 140 CQUAD4 quadrilateral elements along the shell axial dimension, and 204 elements around the shell circumference (Ref. 7), is used to model the monocoque shells. Each finite element is approximately 0.25-in. square, with a unique layup and laminate thickness to define

piecewise continuous approximations to the actual continuous tow steering and overlaps (as necessary) patterns. The contour plot in Figure 6a shows the fiber angles for the first tow-steered ply of both shells, with fiber angles from 10 (purple) to 45 deg. (dark red). The laminate thicknesses for Shell A in Figure 6b range from 8 (blue) to 16 (red) plies, whereas the laminate thicknesses for Shell B (not illustrated) are a constant 8 plies. The laminate midplanes in the Shell A finite element model are shifted radially to maintain a smooth shell inner mold line, which is consistent with the manufacturing process described above.



**a. Ply 3 fiber angle**  **b. Shell A laminate thickness**

**Figure 6. Shell finite element model details.**

Fully clamped boundary conditions are applied to both end planes of the shell, except for the axial displacements at the top plane of the model. These axial displacements are constrained to move together to allow application of a single uniform deflection or point force to that end of the shell. Transverse displacement constraints are also applied to simulate the epoxy potting cast over the shell ends.

To model the imperfect shell geometry, the normalized imperfections described above are superposed on the shell finite element models at a specified rotation angle $\Phi$. The radial coordinate of each node in the shell analysis model is changed from zero (no imperfection) to its corresponding normalized imperfection value. Linear static and bifurcation buckling eigenanalyses are performed in this study to calculate prebuckling axial stiffnesses and buckling loads for these shells. In addition, geometrically nonlinear analyses of the shells are also performed using a modified Riks arc-length method to compute a predicted nonlinear load-displacement response history for the shells. Shell axial stiffnesses and buckling loads are then extracted from the nonlinear load-displacement results.

## 6. Structural Analyses with Normalized Imperfections

To provide baseline values for comparison purposes, finite element models of Shells A and B are analyzed without geometric imperfections, and the resulting prebuckling axial stiffnesses and linear bifurcation buckling loads are listed in Table 2. These reference values agree well with experimental results reported in Table 1, and also with the corresponding linear analysis results for the shells without cutouts presented in Ref. 7.

The four combinations of Shells A and B, and A2 and B2 Imperfections with SF = 1, are analyzed using both linear and geometrically nonlinear FEA. For each of these combinations, a large number of individual analysis cases are run with the geometric imperfections oriented at successive 1.76-deg. increments over the range of rotation angles $\Phi$ = 0 to 180 deg. about the shell

6

longitudinal axis. Results from the analyses performed for each of these cases are presented and discussed in this section.

**Table 2.  Predicted performance of shells without imperfections.**

| Performance metric | Shell A | Shell B |
|---|---|---|
| Prebuckling axial stiffness, klb/in. | 503.87 | 306.87 |
| Buckling load, klbs | 37.35 | 15.65 |

The shell structural performance, computed using linear FEA and normalized by the appropriate reference values from Table 2, is plotted in Figure 7 for rotation angles Φ from 0 to 180 deg. The normalized prebuckling linear axial stiffnesses in Figure 7a exhibit very small variations of less than ±0.2 percent from the corresponding reference values. The associated normalized buckling loads from the linear analyses are shown in Figure 7b, and differ from the reference values by approximately +1 to −3 percent. In addition, over half of the analysis cases evaluated here have buckling loads that are greater than their reference values.

The results from the linear analyses presented here also compare very well qualitatively with the results of similar linear FEA performed in Ref. 7 using measured geometric imperfections. However, quantitative differences of up to 0.1 percent for normalized axial stiffness and 1 percent for normalized buckling load are observed between these two sets of analyses. While relatively small, these differences are most likely due to variations between the measured geometric imperfections used in Ref. 7 and the normalized imperfection data used for the analyses in this study.



a. Axial stiffnesses       b. Buckling loads
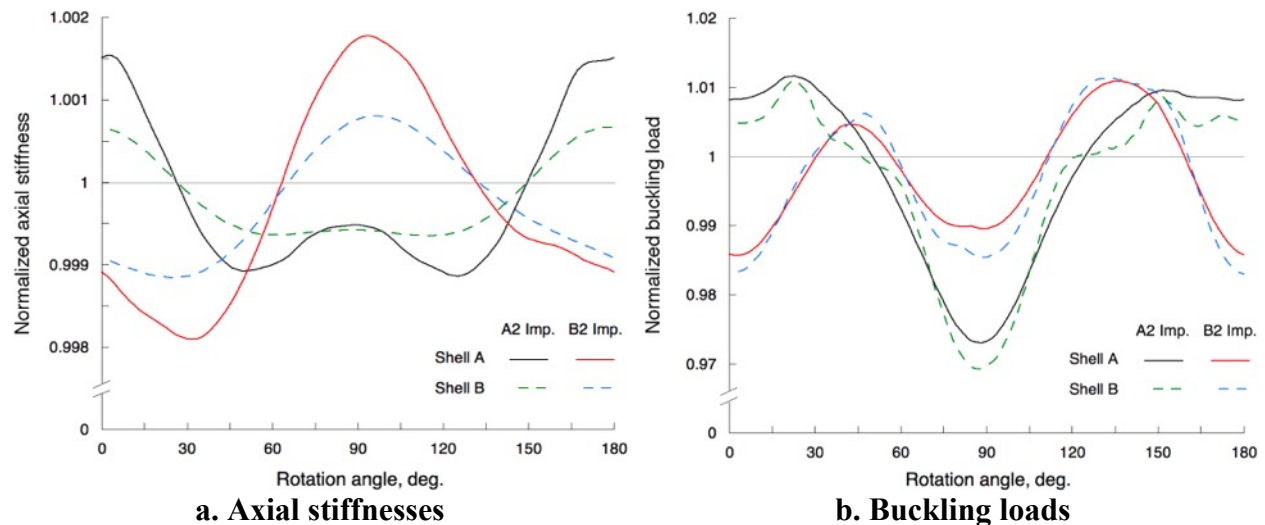
**Figure 7.  Linear structural performance with SF = 1 imperfections.**

The normalized structural performance from the nonlinear analyses of the four shell configurations is plotted in Figure 8. The axial stiffnesses in Figure 8a are qualitatively different from the linear results, and are approximately 1 to 4 percent lower. Sharp localized reductions of up to 1 or 2 percent are also observed in the axial stiffness results. These variations appear as spikes or noise in the plots, and will be discussed in more detail below. The nonlinear buckling loads in Figure 8b show similar qualitative trends to the linear analysis results in Figure 7b, but with generally larger predicted amplitudes that deviate by +1 to −7 percent from the reference

values. As for the axial stiffnesses, similar localized variations of up to 1 or 2 percent are also noted for the nonlinear buckling loads.

The largest differences between linear and nonlinear buckling loads are noted for the Shell A with A2 Imperfections combination, plotted as the black lines in the figures, at rotation angles between 60 and 120 deg. For this shell configuration, the minimum buckling knockdown is observed at approximately $\Phi = 90$ deg., where the predicted normalized buckling load is about 93 percent of the reference analysis value, or 4 percent under the linear analysis value of 97 percent. Examination of the corresponding A2 Imperfections at $\Phi = 90$ deg. in Figure 5a indicates that, at this orientation, the valley-like geometric imperfections are directed radially inward under the axially-stiff shell crown and keel, with the ridge-like bulges oriented radially outward along the axially-soft shell sides.



a. Axial stiffnesses            b. Buckling loads
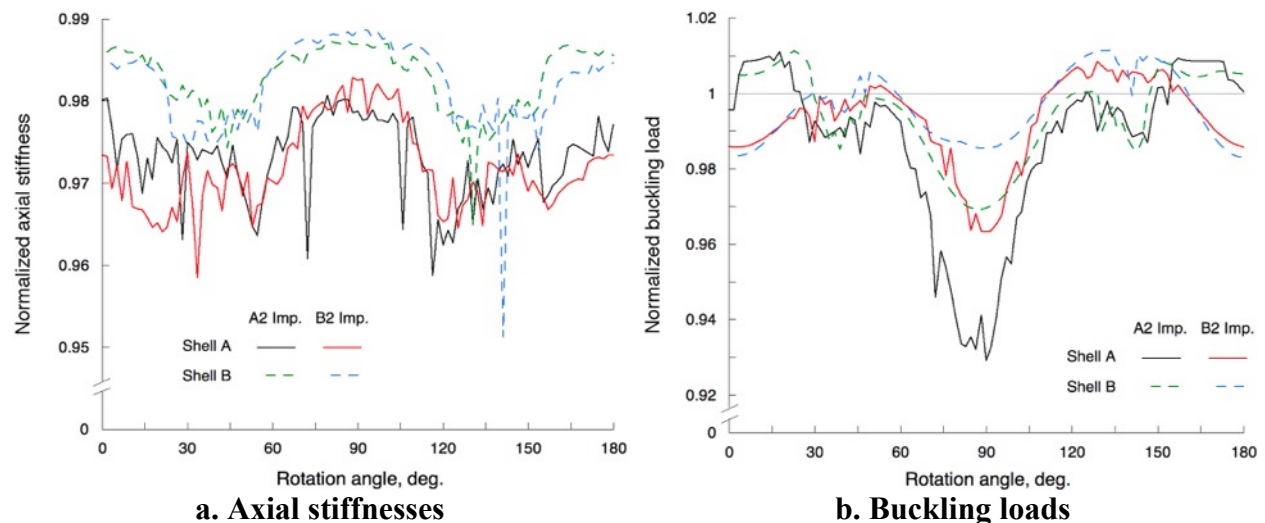
**Figure 8. Nonlinear structural performance with SF = 1 imperfections.**

## 7. Structural Analyses with Scaled Imperfections

To assess the effect of larger geometric imperfection amplitudes on the tow-steered shell structural performance, the A2 and B2 Imperfections with nominal SF = 1 developed and presented previously are amplified photographically using scale factors of SF = 3, 5, and 10. The linear and nonlinear finite element analyses described for the configurations with SF = 1 are then performed using these larger geometric imperfections. As before, the analysis results are normalized using the appropriate values from Table 2 before presentation.

Normalized results from linear structural analyses performed using scale factors of 3, 5, and 10 are plotted in Figures 9, 10, and 11, respectively. The normalized axial stiffnesses for the two intermediate scale factors SF = 3 and 5 show small variations within 0.5 percent from the reference values, but exhibit much larger variations of +1 to –5 percent for the largest SF = 10 imperfections in Figure 11a. The corresponding normalized buckling loads have buckling knockdowns that decrease from 0.90 to 0.70, and are inversely proportional to the scale factor. The percentage of cases with a buckling load that exceeds the reference value also decreases in inverse proportion to the increasing scale factor. Almost none of the cases with SF = 10 have a normalized buckling load greater than 1.
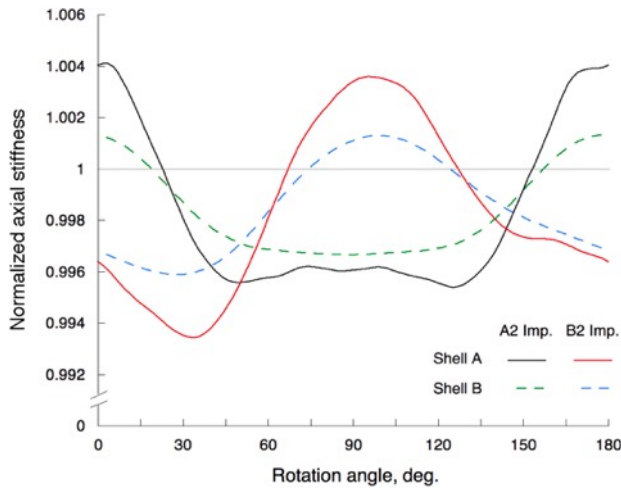
**a. Axial stiffnesses**          **b. Buckling loads**

**Figure 9.  Linear structural performance with SF = 3 imperfections.**
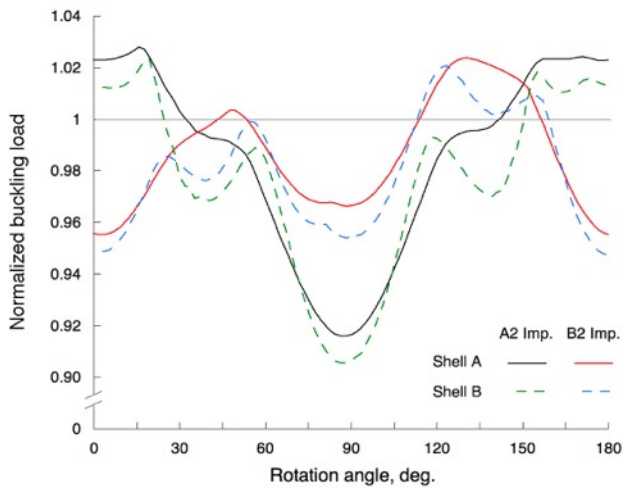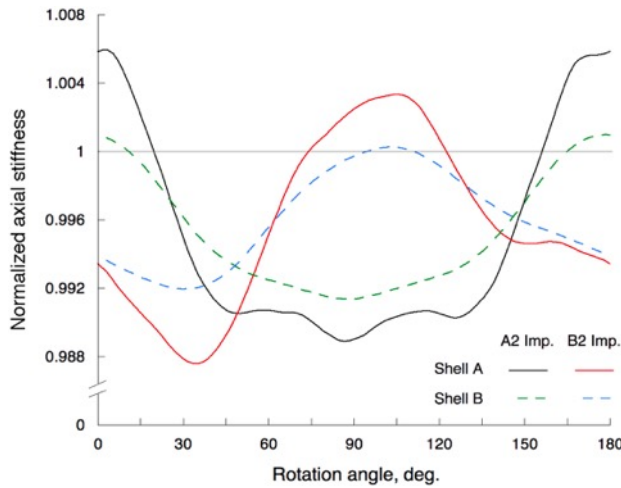


**a. Axial stiffnesses**          **b. Buckling loads**

**Figure 10.  Linear structural performance with SF = 5 imperfections.**
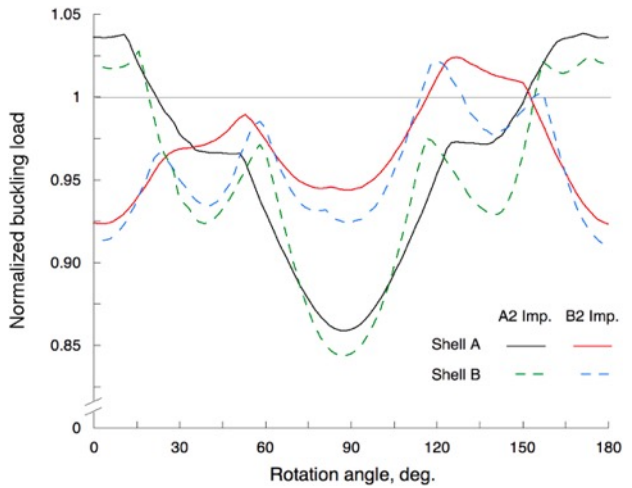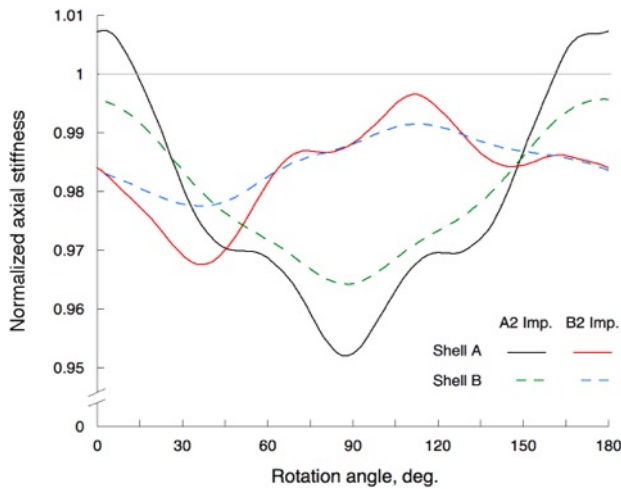


**a. Axial stiffnesses**          **b. Buckling loads**

**Figure 11.  Linear structural performance with SF = 10 imperfections.**
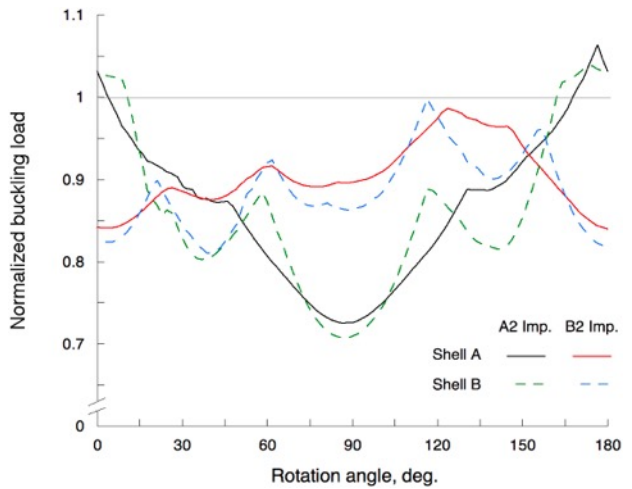
Geometrically nonlinear structural analyses are then performed using the larger imperfection scale factors of SF = 3, 5, and 10. The results of these nonlinear analyses are then normalized to generate the structural performance results presented in Figures 12, 13, and 14, respectively. The sharp, spike-like reductions in axial stiffness noted for SF = 1 in Figure 8a are also evident in the results for the larger scale factors. The largest reductions occur in limited quantities and amplitudes for the smaller scale factors of 3 and 5. However, a larger number of significant reductions are present for many of the cases with SF = 10 imperfections in Figure 14a. In some of the analysis cases studied, the magnitude of these reductions can be as much as 40 percent.

The normalized buckling loads computed from the nonlinear analyses are consistently lower than the corresponding results from the linear analyses plotted in Figures 9 to 11. The small local discontinuities in the buckling load results observed for SF = 1 in Figure 8b are also present for SF = 3 and 5. Sharp local increases in the normalized buckling load with SF = 10 are noted in Figure 14b, and occur at the same rotation angles as the axial stiffness reductions. For the configurations with SF = 10, these increases in buckling load are especially prominent for Shell B with A2 Imperfections for a range of rotation angles between 75 and 105 deg., but are also present (with smaller amplitudes) for Shell A with A2 Imperfections cases analyzed at several other rotation angles.



a. Axial stiffnesses         b. Buckling loads
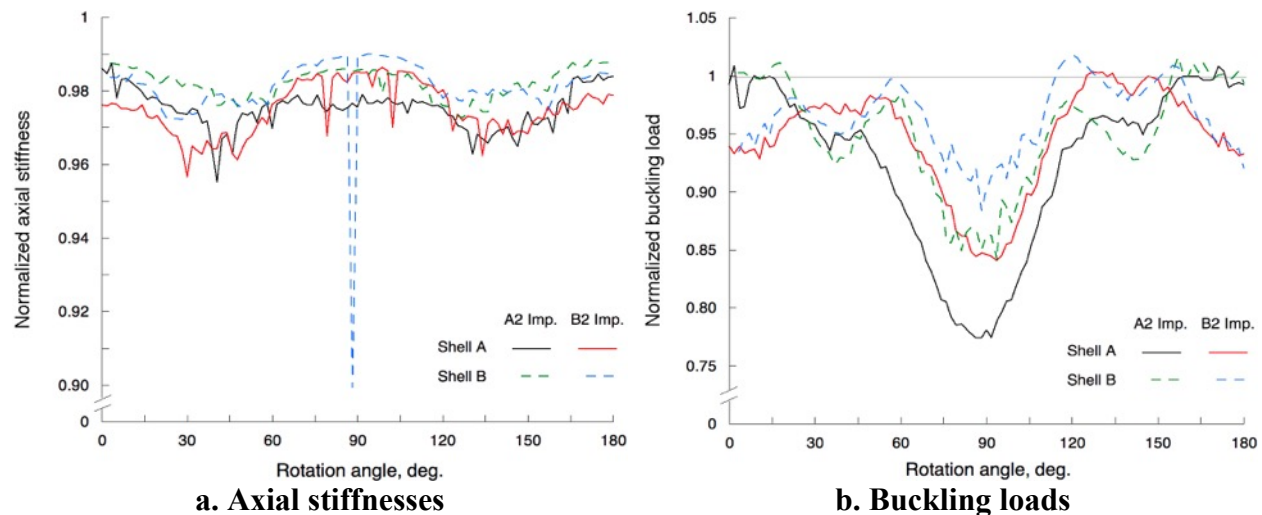
**Figure 12. Nonlinear structural performance with SF = 3 imperfections.**



a. Axial stiffnesses         b. Buckling loads
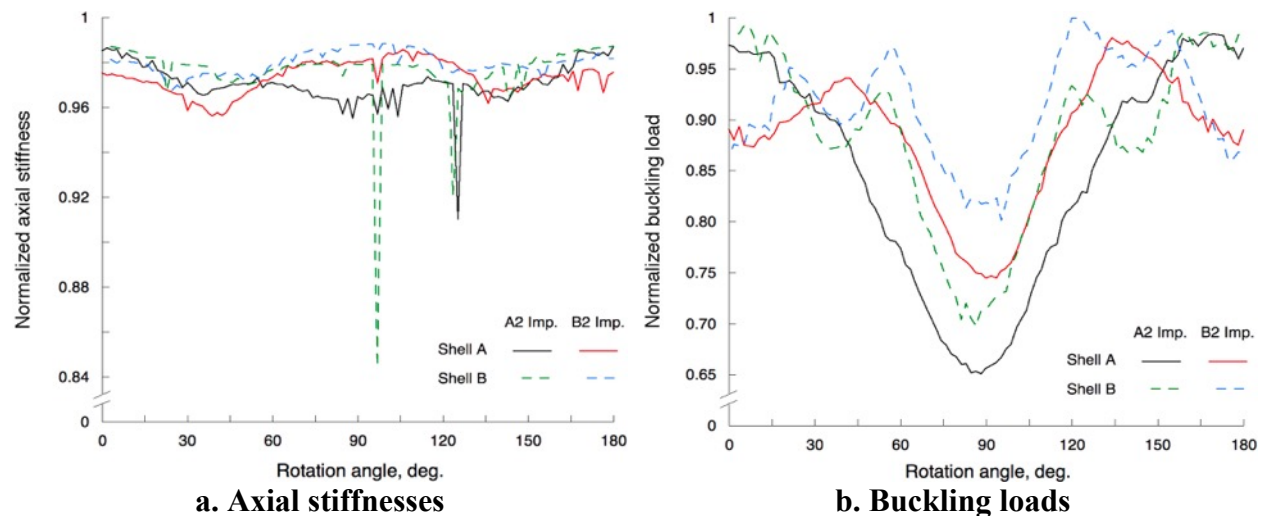
**Figure 13. Nonlinear structural performance with SF = 5 imperfections.**

10

**a. Axial stiffnesses**  **b. Buckling loads**
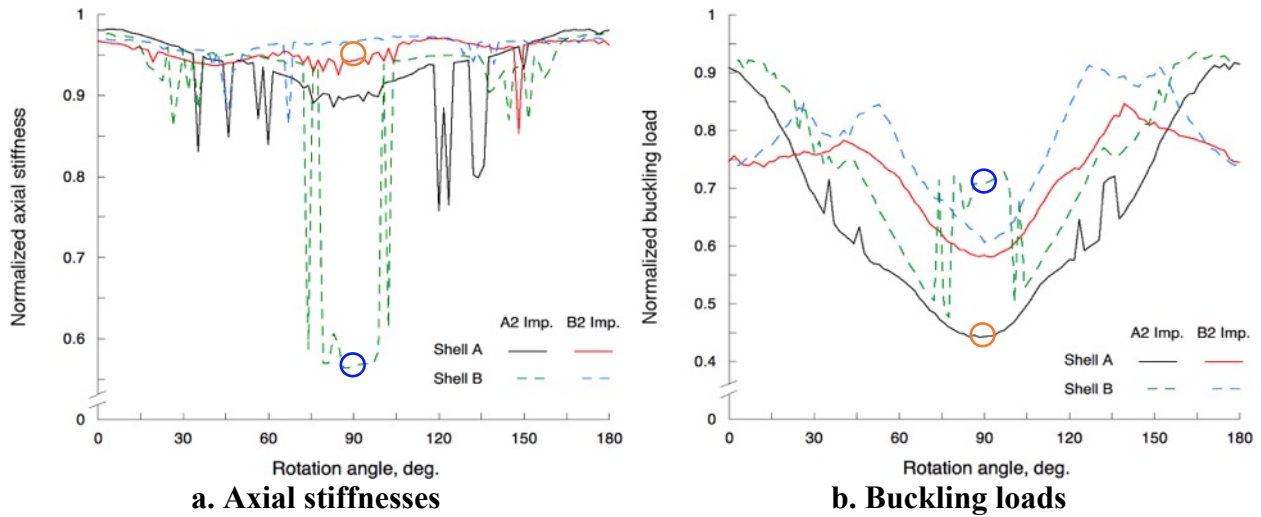
**Figure 14.  Nonlinear structural performance with SF = 10 imperfections.**

## 8.  Detailed Assessment of Nonlinear Analysis Results

One posited cause for the discontinuities noted in the nonlinear analysis results presented above is discussed here, along with a proposed resolution.  An automated batch mode was employed because of the large number of nonlinear analyses generated in this study.  However, running multiple sequential analyses in this batch mode did not allow collection of the full nonlinear load-deflection history for each analysis case.  A MATLAB (Ref. 9) algorithm was developed in this study to more efficiently process the nonlinear analysis output.  This algorithm recovered the maximum value from the load-displacement history (which was assumed to be the buckling load), and divided that load by the corresponding end shortening to calculate the corresponding secant axial stiffness.

This postprocessing method is believed to generate misleading results in some cases, as evidenced by the spikes noted in the nonlinear results above.  Examining one such configuration in more detail, Figure 15 shows the predicted nonlinear load-displacement histories for Shell B and A2 imperfections with SF = 1 and 10 oriented at $\Phi = 90$ deg.  The structural response for the SF = 1 case, plotted as a black solid line, shows classical shell buckling and postbuckling behavior.  This curve shows an initial linear load-displacement response up to a buckling event at 14,920 lbs, followed by a sharp reduction in load and subsequent linear increase in load, up to termination of the analysis at 12,230 lbs.

The nonlinear analysis response for the same shell with SF = 10 is represented by the red dashed line in Figure 15.  This configuration exhibits an initial buckling event at 6940 lbs (indicated by the orange circle in the figure below), and then quickly gains additional load before the analysis ends at 11,100 lbs (the blue circle).  The normalized buckling load and normalized secant stiffness corresponding to this final data point are indicated with blue circles in Figures 14a and 14b, respectively.

To estimate the shell prebuckling axial stiffness from the nonlinear analysis results, a secant stiffness (i.e., load divided by corresponding displacement) is calculated at each converged analysis step up to and including the initial buckling load.  These individual secant stiffnesses are then averaged to estimate the shell axial stiffness for that analysis case.  A secant stiffness calculated using only the initial buckling load, while a much simpler calculation, is consistently lower than this averaged stiffness, as well as the axial stiffness computed from a linear analysis.

Note that the secondary postbuckling stiffnesses are nearly equal for both scale factors in Figure 15.  The load-displacement response of this shell also exhibits a postbuckling behavior with

a nearly plate-like bilinear response. The design of such shells with intentional plate-like postbuckling responses were studied in Ref. 10.
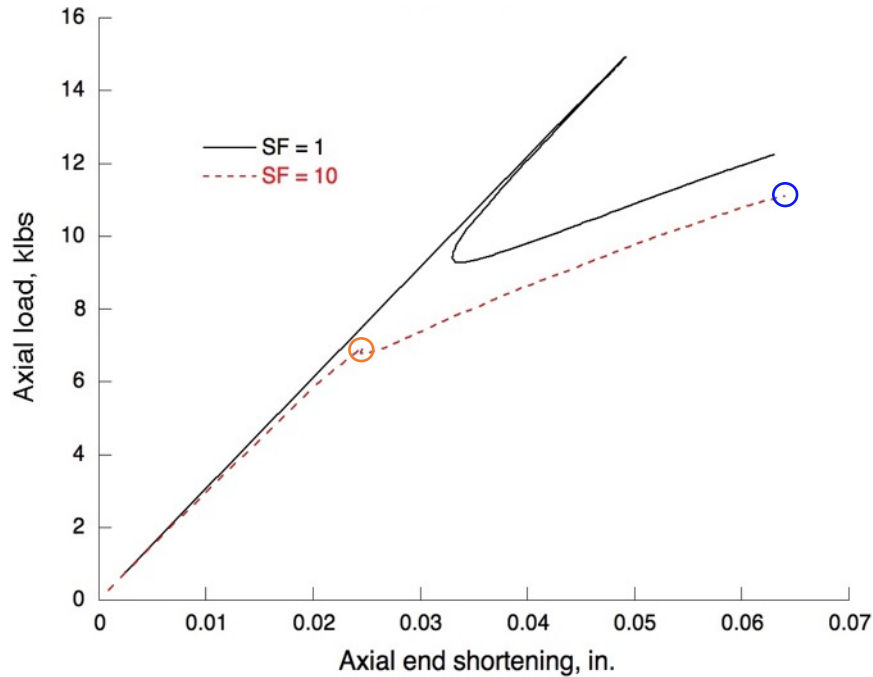


**Figure 15. Nonlinear FEA results for Shell B with A2 Imperfections.**

## 9. Discrete Nonlinear Analysis Results

To provide additional insight into the nonlinear response of the tow-steered shells, detailed nonlinear shell load-displacement responses are calculated for each of the four shell configurations with SF = 1 imperfections at a set of discrete rotation angles $\Phi$ = (0, 30, 60, 90, 120, 150, 180) deg. The (averaged secant) axial stiffnesses and (initial) buckling loads at these discrete angles are normalized by data from Table 2, and then plotted in Figure 16.

The axial stiffness results in Figure 16a show a range of approximately 1.5 percent, and correlate well with the linear analysis results plotted in Figure 7a, which exhibit a much narrower range of approximately 0.4 percent. The axial stiffness trends also agree well with the corresponding nonlinear analysis results in Figure 8a, but the amplitudes are consistently higher by up to 1.5 percent. The buckling loads in Figure 16b extracted from the discrete nonlinear analyses agree qualitatively with the linear analysis results in Figure 7b, and agree both qualitatively and quantitatively when superposed on the nonlinear results in Figure 8b. A direct comparison of the nonlinear analysis results for SF = 1 in Figures 8 and 16 is shown in Figure A1 of Appendix A.

The nonlinear shell load-displacement responses for shell configurations with SF = 3, 5, and 10 imperfections are also analyzed using these same methodologies as described above. The resulting normalized axial stiffnesses and buckling loads from these additional analyses at the same discrete rotation angles are plotted in Figures 17, 18, and 19, respectively.

In each case, the axial stiffnesses from these discrete nonlinear analyses show similar trends as noted for the corresponding nonlinear analysis results plotted in Figures 12a to 14a, but with the higher amplitudes noted for SF = 1. The computed buckling loads in the figures below also show good qualitative and quantitative agreement with the corresponding nonlinear results shown in Figures 12b to 14b, with the exception of the discontinuities noted in Figure 14b for Shell B with A2 Imperfections with SF = 10 at $\Phi$ = 90 deg. The nonlinear analysis results for SF = 3, 5,

and 10 in Figures 12 to 14, and Figures 17 to 19, respectively, are also compared directly in Figures A2 to A4 of Appendix A.
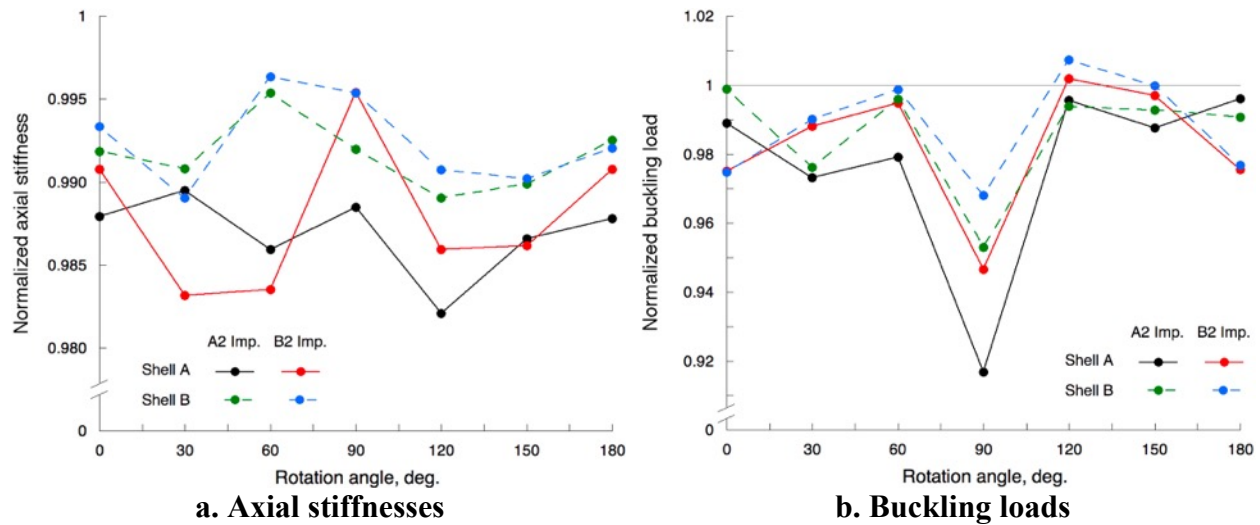


a. Axial stiffnesses
b. Buckling loads

**Figure 16. Discrete nonlinear structural performance with SF = 1 imperfections.**
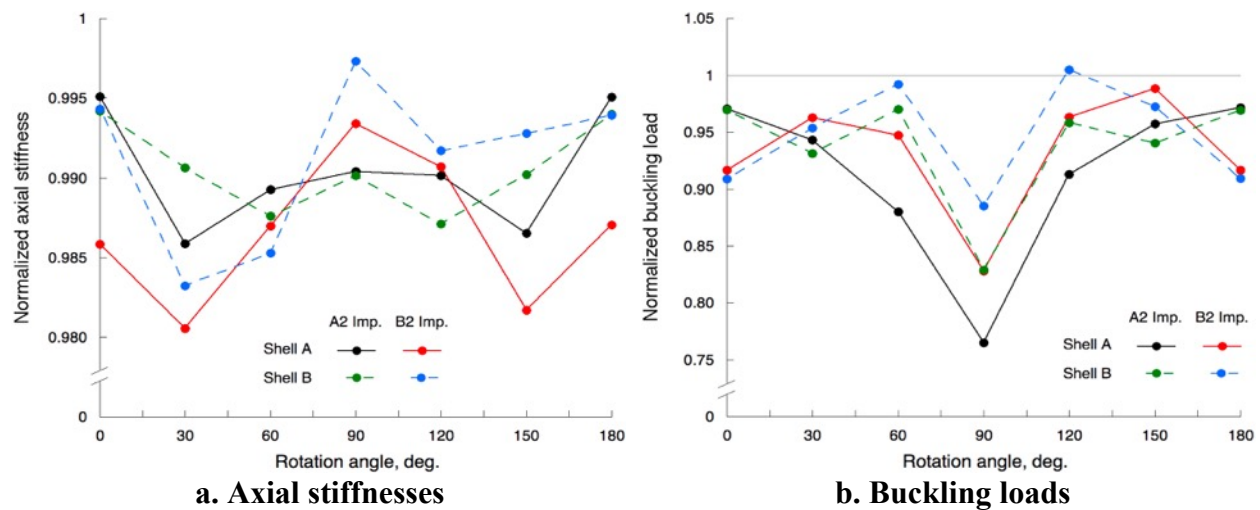


a. Axial stiffnesses
b. Buckling loads

**Figure 17. Discrete nonlinear structural performance with SF = 3 imperfections.**

For SF = 5, several values of axial stiffness and buckling loads for Shell A with B2 Imperfections at rotation angles $\Phi$ = (60, 90, 120, 150, 180) deg., and Shell B with A2 Imperfections at rotation angles $\Phi$ = 150 and 180 deg., were not computed from the nonlinear FEA results. To generate these missing data, the normalized results corresponding to these specific cases are instead interpolated using second-order polynomial curve fits to the associated SF = 1, 3, and 10 data from Figures 16, 17, and 19, respectively. The analyses used to generate these interpolated results are presented in Appendix B. The results of those analyses indicated in Figure 18 as the red open circles for Shell A with B2 Imperfections, and green open circles for Shell B with A2 Imperfections.

The buckling load of 6940 lbs from the nonlinear structural response for Shell B with A2 Imperfections and SF = 10 at a rotation angle $\Phi$ = 90 deg. is designated in Figure 15 with an orange circle. After that buckling load is divided by the corresponding value for Shell B from Table 2, the normalized buckling load is also plotted below using an orange circle in Figure 19b

below, and also in Figure 14b. The associated normalized axial stiffness computed from the nonlinear load-displacement history is also indicated with orange circles in Figures 14a and 19a.



a. Axial stiffnesses          b. Buckling loads
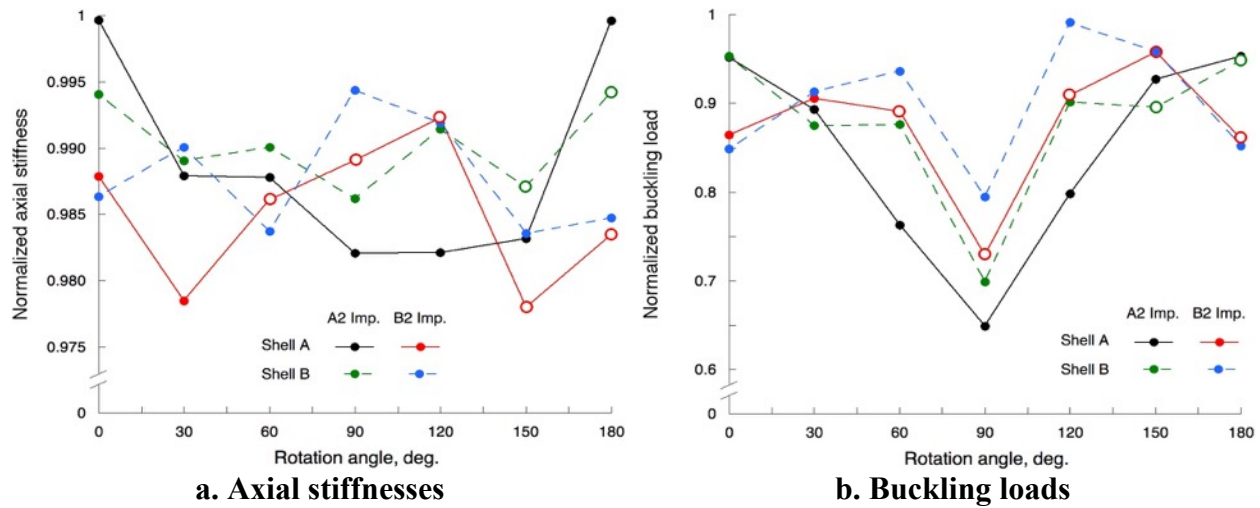
**Figure 18. Discrete nonlinear structural performance with SF = 5 imperfections.**



a. Axial stiffnesses          b. Buckling loads
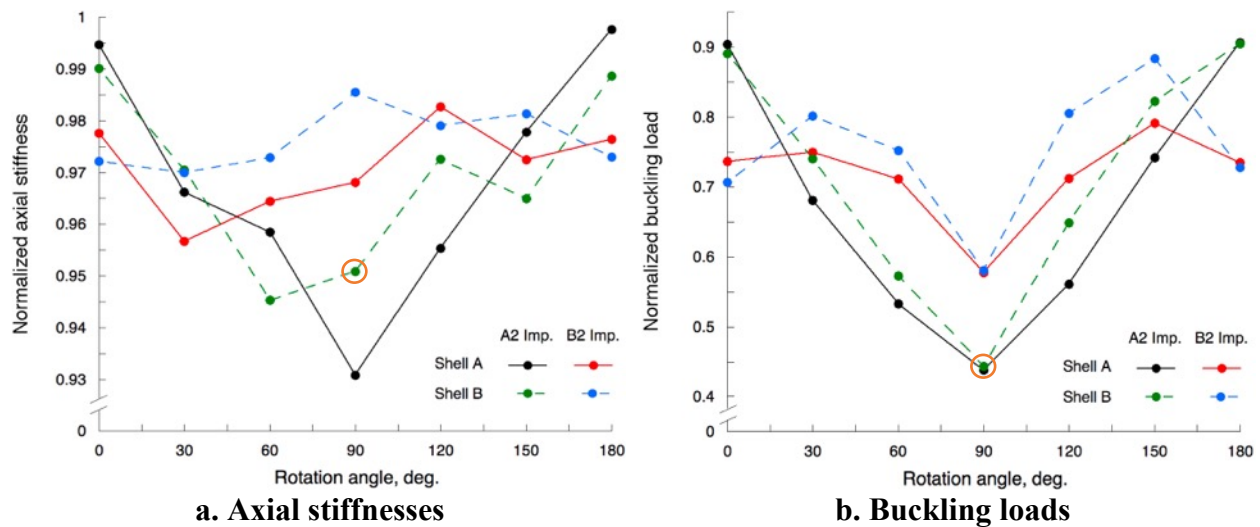
**Figure 19. Discrete nonlinear structural performance with SF = 10 imperfections.**

The average normalized axial stiffnesses for SF = 1, 3, and 5 are approximately within 1 percent of the reference values, with a maximum variation of 2 percent. For SF = 10, the average axial stiffness is 3 percent lower than the reference values, with a maximum variation of 7 percent. The average normalized buckling loads from the nonlinear FEA decrease in inverse proportion to the scale factor, with a maximum reduction for SF = 10 of over 55 percent from the reference values. The computed average (50%), mean minus standard deviation (84.1%), and minimum structural performance values are plotted as functions of the scale factor in Figure 20.

## 10. Concluding Remarks

The structural performance of two advanced composite tow-steered shells are predicted using linear and geometrically nonlinear finite element analyses. Shell analysis models are evaluated without geometric imperfections, and using measured imperfections that are first normalized to ±1 shell wall thickness, and then superposed and rotated incrementally around the shell axis. Using

these nominal imperfections, the shell prebuckling axial stiffnesses and buckling loads are close to reference values from linear analyses with no imperfections.



|  a. Axial stiffnesses | b. Buckling loads |
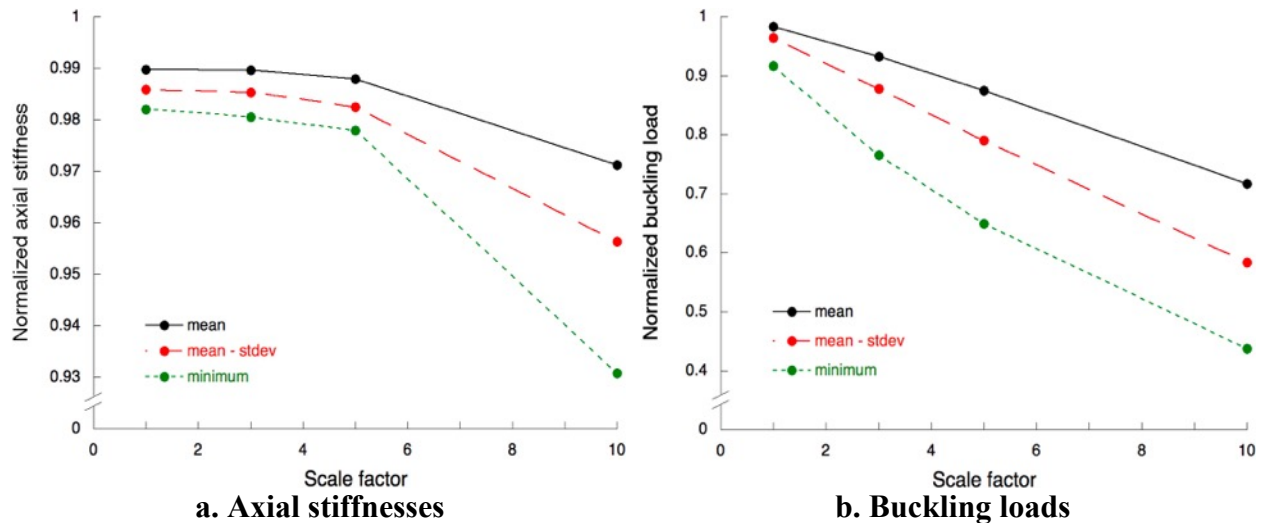
**Figure 20.    Statistical analysis of nonlinear structural performance metrics.**

Shell axial stiffnesses and buckling loads are also evaluated using linear and nonlinear analyses that incorporate normalized imperfections that are scaled up by as much as a factor of 10.  For these larger imperfections, the linear analyses predict reductions in axial stiffnesses and buckling loads of up to 5 and 30 percent, respectively, from the reference values computed without geometric imperfections.  The nonlinear analyses exhibit similar trends, but predict even larger reductions in axial stiffnesses and buckling loads of as much as 10 and 55 percent, respectively, from the reference values.

Possible future work could include expansion of the discrete nonlinear analyses to cover the full range of fiber angles from 0 to 180 degrees.  Hopefully, the axial stiffnesses and buckling loads generated from these additional analyses would not exhibit the same large number of discontinuities noted in the results of this study.  Detailed examination of the linear buckling mode shapes and radial displacements from the nonlinear analyses, their variations, and correlation with buckling loads, could also provide meaningful insight into these tow-steered shells' structural response to compression loads.

### References

1.  D. H.-J. A. Lukaszewicz, C. Ward, and K. D. Potter: *The Engineering Aspects of Automated Prepreg Layup: History, Present and Future.* Composites Part B: Engineering 43.3 (2012): 997-1009.
2.  Z. Gürdal, B. F. Tatting and K. C. Wu: *Variable Stiffness Composite Panels: Effects of Stiffness Variation on the In-Plane and Buckling Response*. Composites Part A: Applied Science and Manufacturing, Vol. 39, No. 5, 2008. Pages 911-922.
3.  K. C. Wu: *Design and Analysis of Tow-Steered Composite Shells Using Fiber Placement*. Proceedings of the ASC 23rd Annual Technical Conference. Memphis, Tennessee, September 9-11, 2008. Paper no. 125.

4. K. C. Wu, B. F. Tatting, B. H. Smith, R. S. Stevens, G. P. Occhipinti, J. B. Swift, D. C. Achary, and R. P. Thornburgh: *Design and Manufacturing of Tow-Steered Composite Shells Using Fiber Placement*. Proceedings of the 50th AIAA/ASME/ASCE/AHS/ASC Structures, Structural Dynamics and Materials Conference. Palm Springs, California, May 4-7, 2009. Paper no. AIAA 2009-2700.

5. K. C. Wu, B. K. Stanford, G. A. Hrinda, Z. Wang, R. A. Martin and H. A. Kim: *Structural Assessment of Advanced Composite Tow-Steered Shells*. Proceedings of the 54th AIAA/ASME/ASCE/AHS/ASC Structures, Structural Dynamics and Materials Conference. Boston, Massachusetts, April 8-11, 2013. Paper no. AIAA 2013-1769.

6. S. C. White, P. M. Weaver, and K. C. Wu: *Post-Buckling Analyses of Variable-Stiffness Composite Cylinders in Axial Compression*. Composite Structures, Vol. 123, May 2015. Pages 190-203.

7. K. C. Wu, B. Farrokh, B. K. Stanford, and P. M. Weaver: *Imperfection Insensitivity Analyses of Advanced Composite Tow-Steered Shells*. Proceedings of the 2016 AIAA Science and Technology Forum and Exposition. San Diego, California, January 4-8, 2016. Paper no. AIAA 2016-1498.

8. Anonymous, MSC Nastran 2012 Quick Reference Guide, MSC Software Corporation, Santa Ana, California, 2011.

9. Anonymous, MATLAB 8.0 and Statistics Toolbox 8.1, The MathWorks, Inc., Natick, Massachusetts, 2012.

10. S. C. White: *Post-Buckling of Variable-Stiffness Shell Structures*. Ph.D. Thesis, University of Bristol, UK, 2016. DOI 10.13140/RG.2.2.28861.46560.

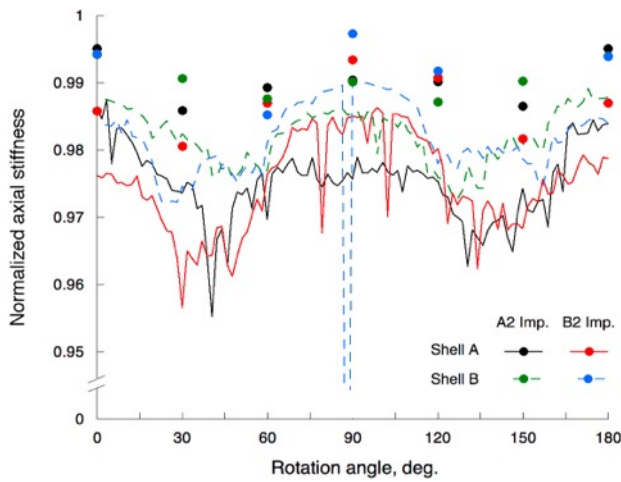# Appendix A.  Comparison of Nonlinear Analysis Results
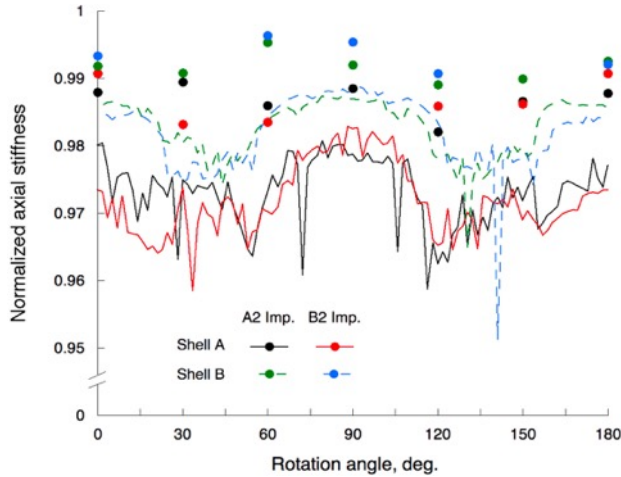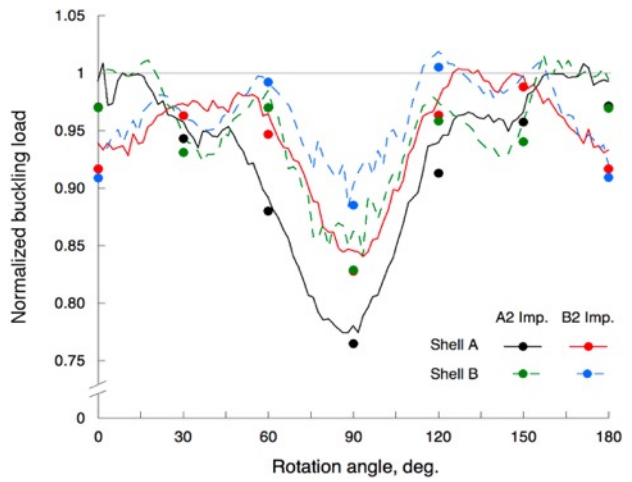


a. Axial stiffnesses
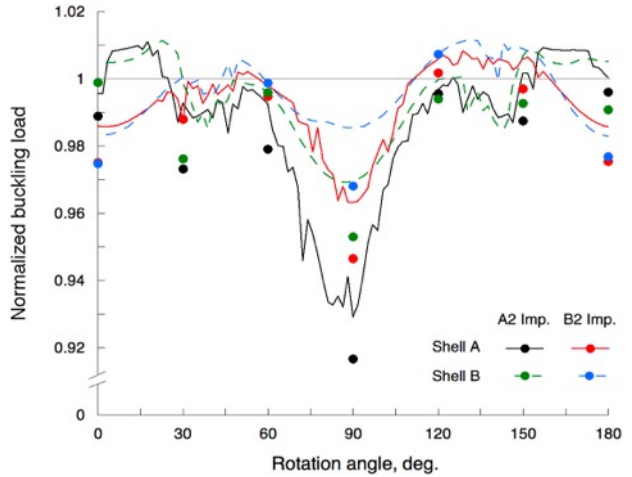
b. Buckling loads

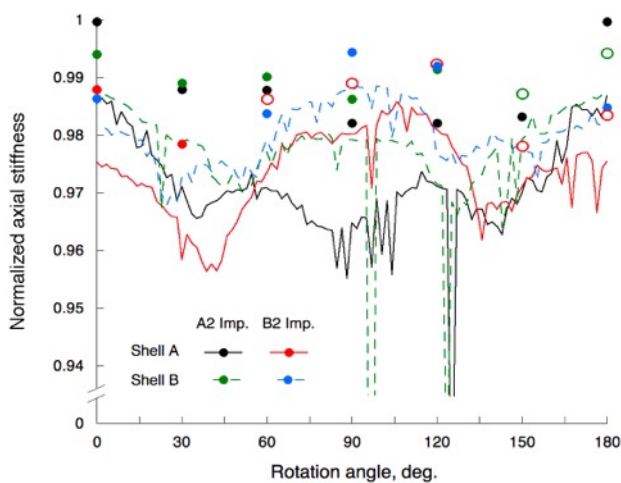Figure A1.  Comparison of nonlinear analyses with SF = 1 imperfections
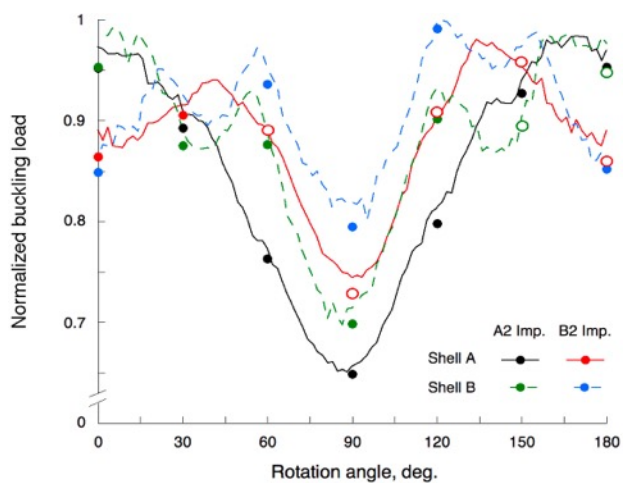


a. Axial stiffnesses

b. Buckling loads

Figure A2.  Comparison of nonlinear analyses with SF = 3 imperfections
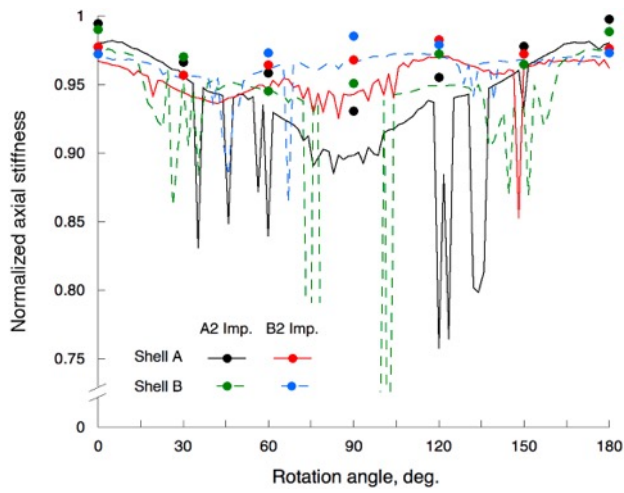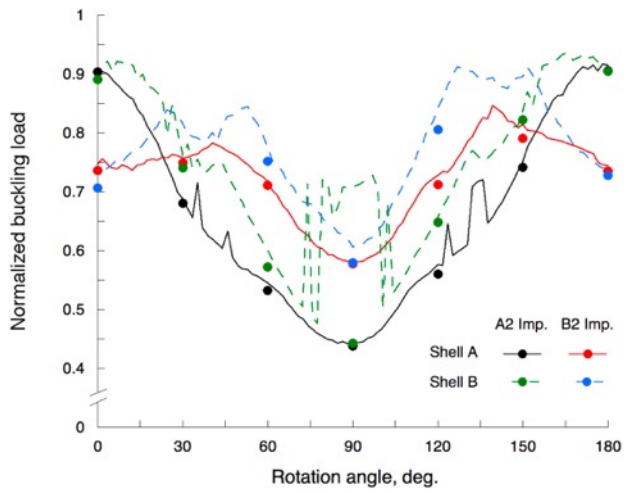


a. Axial stiffnesses

b. Buckling loads

Figure A3.  Comparison of nonlinear analyses with SF = 5 imperfections

a. Axial stiffnesses  b. Buckling loads
Figure A4.  Comparison of nonlinear analyses with SF = 10 imperfections

## Appendix B.  Curve-Fitted Shell Performance Results

Because several normalized axial stiffnesses and initial buckling loads for Shell A and Shell B configurations with SF = 5 are not calculated from the nonlinear FEA, these discrete data are instead interpolated using exact second-order polynomial curve fits to the existing results for SF = 1, 3, and 10 at specified rotation angles.

For Shell A with B2 Imperfections at rotation angles Φ = (60, 90, 120, 150, 180) deg., the normalized structural performance data from the geometrically nonlinear FEA in Figures 16, 17, and 19 are indicated with the filled circles in Figure B1, and the polynomial curve fits to these discrete data are superposed as solid lines.  The interpolated results at SF = 5 are indicated with the open circles in Figure B1, and are then exported to Figure 18 as the red filled circles.
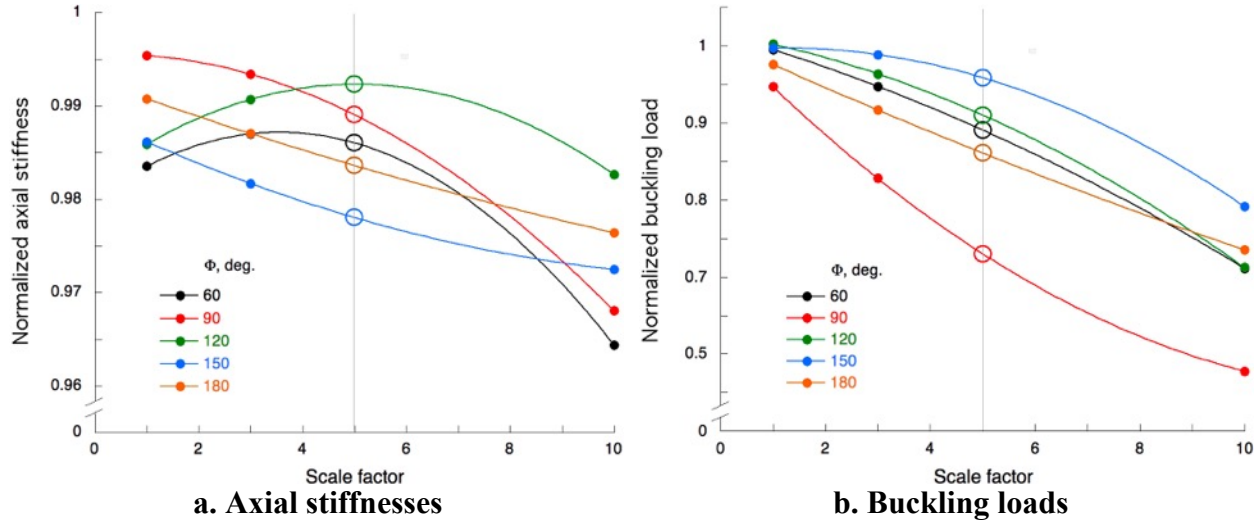


a. Axial stiffnesses                              b. Buckling loads
**Figure B1.  Interpolated performance for Shell A with B2 Imperfections.**

The corresponding curve-fitted structural performance for Shell B with A2 Imperfections at rotation angles Φ = 150 and 180 deg. are illustrated in Figure B2.  The normalized structural performance data from Figures 16, 17, and 19 are plotted as the filled circles, with the curve fits again shown as solid lines.  The estimated values at SF = 5 are plotted as the open circles in Figure B2, and are replotted as the green filled circles in Figure 18.
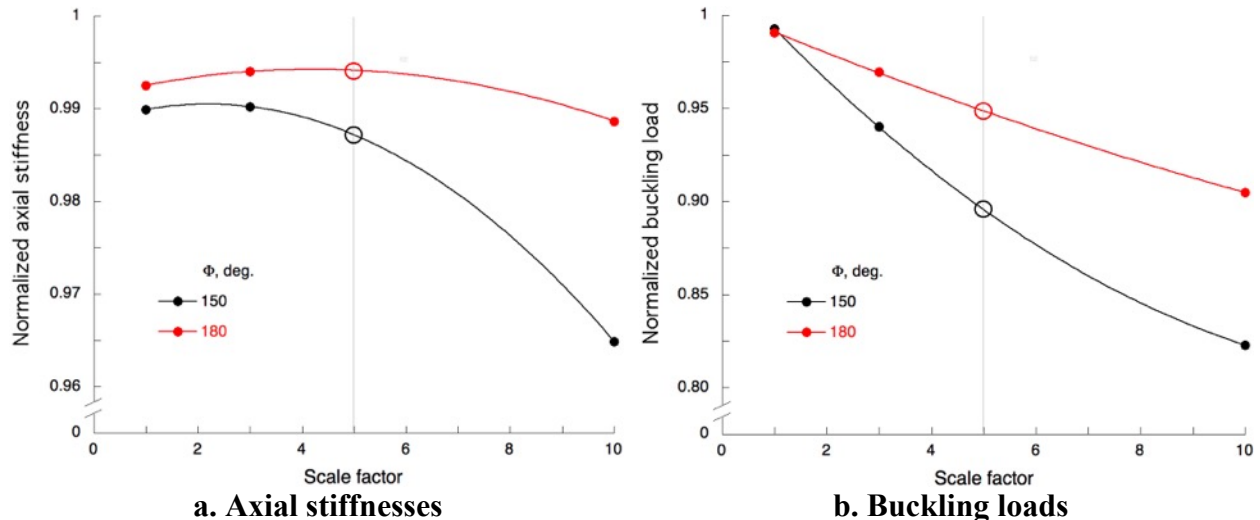


a. Axial stiffnesses                              b. Buckling loads
**Figure B2.  Interpolated performance for Shell B with A2 Imperfections.**

19

# REPORT DOCUMENTATION PAGE

| 1. REPORT DATE (DD-MM-YYYY)<br>1-10-2019 | 2. REPORT TYPE<br>Technical Memorandum | 3. DATES COVERED (From - To) |
|---|---|---|

**4. TITLE AND SUBTITLE**

Preliminary Nonlinear Structural Analysis of Advanced Composite Tow-Steered Shells with Large Geometric Imperfections

**5a. CONTRACT NUMBER**

**5b. GRANT NUMBER**

**5c. PROGRAM ELEMENT NUMBER**

**6. AUTHOR(S)**

Dobrin, Calvin P.; Wu, K. Chauncey; Stanford, Bret K.

**5d. PROJECT NUMBER**

**5e. TASK NUMBER**

**5f. WORK UNIT NUMBER**
432938.11.01.07.43.40.08

**7. PERFORMING ORGANIZATION NAME(S) AND ADDRESS(ES)**

NASA Langley Research Center
Hampton, VA 23681-2199

**8. PERFORMING ORGANIZATION REPORT NUMBER**

L-21065

**9. SPONSORING/MONITORING AGENCY NAME(S) AND ADDRESS(ES)**

National Aeronautics and Space Administration
Washington, DC 20546-0001

**10. SPONSOR/MONITOR'S ACRONYM(S)**

NASA

**11. SPONSOR/MONITOR'S REPORT NUMBER(S)**
NASA-TM-2019-220413

**12. DISTRIBUTION/AVAILABILITY STATEMENT**

Unclassified-
Subject Category 02
Availability: NASA STI Program (757) 864-9658

**13. SUPPLEMENTARY NOTES**

**14. ABSTRACT**

The structural performance of two advanced composite tow-steered shells with and without tow overlaps, and with large geometric imperfections, are predicted using linear and geometrically nonlinear finite element analyses. These shells, 35 in. long and approximately 16.3 in. diameter, are fabricated using automated fiber placement from IM7/8552 graphite/epoxy prepreg. The 8-ply, $[\pm 45/\pm Q]$s shell layup incorporates a steered fiber angle Q that varies from 10 deg. to 45 deg. periodically over the shell circumference. Shell analysis models are evaluated using geometric imperfections normalized to $\pm 1$ shell wall thickness ($\pm 0.040$ in.), which are then superposed and rotated incrementally around the shell longitudinal axis. Using these nominal imperfections, the shell prebuckling axial stiffnesses and buckling loads predicted with linear and nonlinear analyses are close to reference values from linear analyses with no imperfections. The linear and nonlinear analyses are then repeated for scaled imperfections that are larger by up to a factor of 10. For these larger imperfections, linear analyses predict reductions in axial stiffnesses and buckling loads of up to 5 and 30 percent, respectively, from reference values. The nonlinear analyses predict even larger reductions in axial stiffnesses and buckling loads of up to 10 and 55 percent, respectively.

**15. SUBJECT TERMS**

Advanced Composite; Composite Structures; Tow-Steered Shells

| 16. SECURITY CLASSIFICATION OF: | | | 17. LIMITATION OF ABSTRACT | 18. NUMBER OF PAGES | 19a. NAME OF RESPONSIBLE PERSON |
|---|---|---|---|---|---|
| a. REPORT | b. ABSTRACT | c. THIS PAGE | | | STI Help Desk (email: help@sti.nasa.gov) |
| U | U | U | UU | 24 | **19b. TELEPHONE NUMBER** (Include area code)<br>(757) 864-9658 |